AIAA 2002-2794
Uncertainty of Videogrammetric Techniques used for Aerodynamic Testing

A. W. Burner, Tianshu Liu, Richard DeLoach
NASA Langley Research Center
Hampton, VA

**22nd AIAA Aerodynamic
Measurement Technology and
Ground Testing Conference
24-26 June, 2002
St. Louis, Missouri**

Uncertainty of Videogrammetric Techniques used for Aerodynamic Testing

A. W. Burner[*], Tianshu Liu[†], Richard DeLoach[‡]
NASA Langley Research Center
Hampton, VA 23681-2199

ABSTRACT

The uncertainty of videogrammetric techniques used for the measurement of static aeroelastic wind tunnel model deformation and wind tunnel model pitch angle is discussed. Sensitivity analyses and geometrical considerations of uncertainty are augmented by analyses of experimental data in which videogrammetric angle measurements were taken simultaneously with precision servo accelerometers corrected for dynamics. An analysis of variance (ANOVA) to examine error dependence on angle of attack, sensor used (inertial or optical), and on tunnel state variables such as Mach number is presented. Experimental comparisons with a high-accuracy indexing table are presented. Small roll angles are found to introduce a zero-shift in the measured angles. It is shown experimentally that, provided the proper constraints necessary for a solution are met, a single-camera solution can be comparable to a 2-camera intersection result. The relative immunity of optical techniques to dynamics is illustrated.

INTRODUCTION

As demand and usage increases for a particular test technique, issues related to the uncertainty of the measurement technique become more important. For instance, it is not uncommon for better accuracy to be desired as a given technique is used more and more. This has certainly been the case for pitch angle measurements in wind tunnels where the desired accuracy has slowly changed through the years down to less than 0.01° for some applications. Possible new uses of the data from the technique may also arise, once the data is available on a nearly routine basis, that may either require better accuracy or the use of the measurement technique in a different mode. Thus not only is the accuracy of a given technique of

fundamental importance, but, in addition, the sensitivity of the technique to variations in setup geometry, etc. are of interest to assess the possible loss in accuracy that might be necessary to accommodate unique requirements. The importance of supplementing uncertainty analyses with experimental error assessments and the use of modern design of experiments methods (MDOE) has been emphasized in reference 1.

Videogrammetric techniques combine photogrammetry, solid-state area-array cameras and image processing to yield rapid spatial measurements. Videogrammetric techniques have been used at a number of NASA facilities, primarily for the measurement of static aeroelastic model deformation[2]. Variations of videogrammetric techniques include single-camera and multiple-camera implementations, depending on the nature of the application[3]. For example, a single-camera, single-view implementation at the Langley National Transonic Facility (NTF) has been used for the last ten customer tests. A typical image used for measurements at the NTF is presented in figure 1. For most of these tests model static aeroelastic data were obtained for nearly every data point acquired throughout the test, resulting in many thousands of data points of static aeroelastic data per test such as the typical example in figure 2. The interest and demand by industry for these aeroelastic measurements has increased dramatically as the technique has been improved without compromising facility productivity. A more complete and thorough uncertainty analysis will improve the value of this deformation data supplied to industry. More recent investigations with videogrammetric techniques include the measurement of aerodynamic loads[4], developments for use with micro air vehicles (both fixed- and flapping-wing), for ultra-light and inflatable large space structures during and after deployment[5], and for in-flight aeroelastic measurements. Techniques are also under study for laboratory and wind tunnel dynamic measurements at frequencies up to 1000 Hz.

The second aerodynamic measurement to be considered is pitch angle measurement, which is a fundamental measurement requirement of all wind tunnels. Note

---

* Senior Research Scientist, Senior Member
† Research Scientist, Member
‡ Senior Research Scientist, Member

correction requires iteration with x_d, y_d as start values to determine the final distortion correction iteratively. The asymmetrical (or decentering) terms δx_a, δy_a in (3) are given by

$$\delta x_a = P_1\left(r^2 + 2x^2\right) + 2P_2 x\, y$$
$$\delta y_a = P_2\left(r^2 + 2y^2\right) + 2P_1 x\, y \tag{5}$$

The collinearity equations can be recast in linear form as

$$a_1 X + a_2 Y + a_3 Z = a_1 X_c + a_2 Y_c + a_3 Z_c$$
$$a_4 X + a_5 Y + a_6 Z = a_4 X_c + a_5 Y_c + a_6 Z_c \tag{6}$$

If 2 or more cameras image a single point and a_1 through a_6 (containing coefficients x_p, y_p, c, ω, ϕ, κ) and X_c, Y_c, Z_c are known, then the spatial coordinates X, Y, Z can be determined with linear least squares. If one of the spatial coordinates is known such as Y, then a single camera image of a point results in 2 equations in 2 unknowns. With Y known, X and Z can be found from

$$X = X_c + \frac{(Y - Y_c)(a_2 a_6 - a_5 a_3)}{(a_4 a_3 - a_1 a_6)}$$
$$Z = Z_c - \frac{(X - X_c)a_1 + (Y - Y_c)a_2}{a_3} \tag{7}$$

Where

$$a_1 = \left(x - x_p\right)m_{31} + c\, m_{11}$$
$$a_2 = \left(x - x_p\right)m_{32} + c\, m_{12}$$
$$a_3 = \left(x - x_p\right)m_{33} + c\, m_{13}$$
$$a_4 = \left(y - y_p\right)m_{31} + c\, m_{21} \tag{8}$$
$$a_5 = \left(y - y_p\right)m_{32} + c\, m_{22}$$
$$a_6 = \left(y - y_p\right)m_{33} + c\, m_{23}$$

Once the X and Z coordinates are computed for a given semispan location, a slope angle is computed in the XZ plane by either least squares, or directly when there are only 2 targets per semispan as is the usual case at the NTF. This angle, designated as the raw videogrammetric angle θ_{raw}, is given at each semispan η by

$$\theta_{raw}(\eta) = \tan^{-1} \frac{\Delta Z_\eta}{\Delta X_\eta} \tag{9}$$

A 3rd order polynomial correction (based on the onboard accelerometer used to determine model pitch angle with wind-off or at low Mach number) is then applied to θ_{raw} to yield the corrected angle θ. The polynomial correction at each semispan station is given by

$$\theta = b_0 + b_1 \theta_{raw} + b_2 \theta_{raw}^2 + b_3 \theta_{raw}^3 \tag{10}$$

The b_0 term serves to zero the angle at $0°$ pitch angle. The other terms b_1 through b_2 correct for any (normally small) scale differences and nonlinearity when compared to the onboard accelerometer used for pitch angle measurements. These correction coefficients are determined for each run series to partially account for slight instrumentation and/or facility bias changes with time. A pair of reference runs, one before the run set and one after, are made with wind off or, in the case of the NTF, at low mach number such as $M = 0.1$. Polynomial correction coefficients are determined for each semispan station over the range of expected pitch angles. The change in twist $\Delta \theta$ is computed as the difference in θ between wind-off and wind-on or

$$\Delta \theta = \theta_{on} - \theta_{off} - \Delta \theta_{(\eta \sim 0)} \tag{11}$$

where θ_{off} is taken to be the model pitch angle without flow angularity. The term $\Delta \theta_{(\eta \sim 0)}$ in (11) is the apparent or real difference between the body local angle measured with videogrammetry and the accepted pitch angle. The angle θ_{off} has an additional correction applied at the NTF to account for reference runs being made with flow at low Mach number. This additional correction is based upon the nearly linear relationship between the change in wing twist and the lift coefficient c_l and the dynamic pressure normalized by the modulus of elasticity, or q/e. These additional corrections are a function of semispan location. Load coefficients are initially estimated from best guesses of the wing twist versus dynamic pressure. After wing twist data have been acquired and analyzed during the early part of a given test, the load correction coefficients are updated and the previous data re-reduced. The load sensitivity coefficients at each semispan are given by

$$D_\eta = \frac{\Delta \theta_\eta}{\frac{q}{e} c_l} \tag{12}$$

camera at the positions 1 and 2, respectively. As shown in figure 5, the angular uncertainty $d\theta$ is reduced by compensating the camera principal distance at different positions. Another case of interest is when the camera moves along the X-direction. Figure 6 shows the angular uncertainty $d\theta$ as a function of X_c with and without compensation of the camera principal distance c. Figure 7 shows the angular uncertainty $d\theta$ as a function of ω as the camera moves around the model. Figures 8-11 show the angular uncertainty $d\theta$ as a function of ϕ, κ, x_p, and K_1. In the single-camera solution, it is assumed that the spanwise location Y of the targets is a given constant. However, in actual measurements, the given spanwise location Y of the targets may not be accurate. When there is an error in the given location Y, errors occur in X and Z. The angular uncertainty $d\theta$ is plotted in figure 12 as a function of dY for different values of ω. Note that the angular error caused by dY can be partly thought of as a bias error that is largely reduced by zeroing. In addition a systematic error that is produced by dY and that varies as a function of the angle can be lessened considerably by the use of reference polars to calibrate the videogrammetric system in terms of known angles.

REFERENCE POLAR ANALYSIS
Reference polars are made periodically to calibrate the videogrammetric measurement system in terms of the onboard accelerometer used for precision pitch angle measurements. The change in zero-shift as a function of run set number for a recent test at the National Transonic Facility is plotted in figures 13 and 14. This data represents calibration data for over 3500 data points over a 2.5-month interval. The data is plotted for each of the 6 semispan stations where deformation data were acquired. The inboard station at $\eta = -0.05$ was used to remove angular sting bending and any bias error common to all semispan stations. The relatively large change in zero-shift evident at $\eta = 0.77$ and 0.92 occurred due to a part change with corresponding new targets at different local angles. Two targets were present at each semispan station η. Target spacing varies from 6 inches at $\eta = -0.05$ to less than 2 inches at $\eta = 0.99$. Although the change in zero-shift inboard is less than 0.1° throughout the 2.5 month test, changes in zero-shift near the tip approached 1 degree. Similar plots for the 1st, 2nd, and 3rd-order terms are given in figures 15 to 20. For those plots the correction computed at an α of 6° is shown. The changes in zero-shift at the various η stations are plotted versus total temperature T_t and total pressure P_t in figures 21 to 24. There appear to be no dramatic correlations with temperature or pressure. Thermal expansion and contraction of the test section that may lead to a non-

repeatable orientation in pitch of the video CCD camera may not necessarily be the cause of the zero-shift since that type of orientation change should be observed at all semispan stations (especially for $\eta = -0.05$ and $\eta = 0.35$) which is not reflected in the data plots. The values of zero-shift and slope change of the videogrammetric calibration data should be compared to precision servo-accelerometers, which typically have a zero-shift of less than 0.01° and a slope change (at $\alpha = 6°$) of 0.001° or less over several months[14].

ARC LENGTH EFFECT
Wing bending causes the Y coordinate of wing targets to decrease which causes a bias error in the computation of X and Z if not properly accounted for. Consider the case for simple beam bending given by

$$\Delta Z = c_1 Y^2 + c_2 Y^3 \qquad (21)$$

If we approximate wing bending by (21), an arc length computation can be used to estimate the amount of shift as a function of Y. Denoting the variable of integration by t^*, the arc length $s(t)$ is given by[6]

$$s(t) = \int_0^t \sqrt{\dot{r}\dot{r}}\, dt^* \qquad (22)$$

where
$$\dot{r} = \frac{dr}{dt^*} \qquad (23)$$

With unit vectors $\hat{i}$ and $\hat{j}$ in the Y and Z directions respectively, the vector $\vec{r}$ can be written

$$\vec{r} = t\hat{i} + (c_1 t^2 + c_2 t^3)\hat{j} \qquad (24)$$

so that

$$\dot{r} = \hat{i} + (2c_1 t + 3c_2 t^2)\hat{j} \qquad (25)$$

For small deflections the integrand in (22) can then be approximated making use of the binomial formula for the result for $\sqrt{\dot{r}\dot{r}}$ to yield

$$s(t) \approx \int_0^t (1 + 2c_1^2 t^2 + 3c_1 c_2 t^3 + \frac{9}{2}c_2^2 t^4)\, dt^* \qquad (26)$$

which can be evaluated to become

accelerometer[9]. One of the two stingwhip-corrected accelerometer outputs was used as a reference upon which to base differential pitch measurements made with all the other instruments under study. This eliminated angle of attack set point error from the unexplained variance, which permitted much more subtle effects to be resolved with the correspondingly lower noise level. This choice of a reference was based on the fact that precision servo accelerometers represent the current state of the art in wind tunnel pitch angle measurements.

The Mach number set-point order was randomized within each block to increase the degree of statistical independence in the data and thereby defend against the effects of systematic variations due to such factors as drift in the instrumentation and data systems, changes over time in flow angularity and wall-effects, and various effects attributable to systematic temperature variations, etc.[10-12]. At each Mach number, nominal set-point angles of $-4°$ to $+10°$ in $2°$ steps were acquired in random order to further defend against the effects of any systematic variations that might have been in play while data were acquired at a given Mach number. Figure 27 displays the temperature time history over the time the sixteen wind-on runs were acquired. This figure illustrates systematic changes in tunnel temperature over periods of time in which individual (randomized) polars were acquired, and even wider systematic temperature variations from Mach number to Mach number. The randomization is intended to decouple Mach and pitch angle effects from any systematic error that could be induced by such temperature variations, or other systematic error effects.

Analysis of Variance Tables I and II present the results of an analysis of variance (ANOVA) conducted on the wind-off and wind-on data, respectively. The variables A, B, and C in the wind-off ANOVA represent angle of attack, run – a surrogate for elapsed time (pre-test, mid-test, or post-test), and instrument, respectively. The B and C variables were treated as categorical (discrete-level) variables (three runs and four instruments – the two servo accelerometers and two videogrammetric systems) while angle of attack was treated as numeric (continuous), and modeled to first order. Therefore the "A" variable in Table I represents the slope of pitch error regressed against angle of attack set point.

For the wind-on ANOVA table, A and C are again angle of attack and instrument, respectively, but the B variable now represents Mach number. Angle of attack was treated as numeric. The high precision afforded by MDOE blocking techniques that minimized set-point error and systematic variations permitted terms in a wind-on angle of attack model as high as 4th-order to be

resolved in the presence of the remaining unexplained variance. See Table II. The wind-on B and C variables were treated as categorical variables. There were four discrete Mach numbers (0, 0.3, 0.8, and 0.9) and six pitch instruments. In addition to the two servo accelerometers and two videogrammetric systems used in the wind-off ANOVA, the wind-on ANOVA added pitch estimated from the arc sector corrected for sting bending, and the stingwhip-corrected output of the servo accelerometer not being used as a reference for the differential wind-on pitch measurements.

The wind-off ANOVA in Table I reveals statistically significant main effects for angle of attack, elapsed time, and instrument, as well as a significant interaction between elapsed time and instrument. The "F-value" is relatively high for each of these factors. This represents the portion of explained variance attributable to a given source, normalized by the unexplained variance. The "prob > F" column of the ANOVA table indicates the probability that an F-value this large could occur from ordinary chance variations in the data. Small values imply that it is unlikely that the effect could appear so great by chance alone, and that therefore there is a high probability that the effect is not due to chance but is in

Table I: Wind-off ANOVA

Source	Sum of Squares	DF	Mean Square	F Value	Prob > F
Model	0.009039	17	0.000532	38.7	< 0.0001
A	6.54E-05	1	6.54E-05	4.8	0.0317
B	0.004477	2	0.002239	163.0	< 0.0001
C	0.002826	3	0.000942	68.6	< 0.0001
AB	1.01E-05	2	5.06E-06	0.4	0.6929
AC	5.79E-05	3	1.93E-05	1.4	0.2469
BC	0.001603	6	0.000267	19.4	< 0.0001
Residual	0.001236	90	1.37E-05		
LOF	0.00119	78	1.53E-05	3.9	0.0059
PE	4.66E-05	12	3.89E-06		
Cor Total	0.010276	107			

fact real. If "prob > F" is less than 0.05, for example, then we can say with at least 95% confidence that the associated effect is real, and not an artifact of experimental error in the data. Note that "prob > F" is very small for the A, B, and C main effects in the wind-off data, and for the BC two-way interaction.

The ANOVA table can indicate roughly the relative size of the explained (significant) effects. Note, for example, that the largest F-value in the wind-off data occurs for variable B, which is run number. This implies that averaged across all instruments and all angles of attack in the experiment, the pitch error

angle of attack. Finally, there was a significant quartic angle of attack term that did not interact with B, C, or BC.

The significant higher order angle of attack terms in the wind-on data indicates that delta-pitch varied in a complex way with angle-of-attack set point when the wind was on. The fact that these higher-order terms exhibited interactions with the B and C variables (Mach number and instrument) indicate that the complex angle of attack dependence depended on instrument and Mach number. Figures 31, 32, and 33 illustrate this.

Figure 34 reveals the effects of stingwhip on conventional servo-accelerometers, which has motivated interest in the possible application of videogrammetric methods to pitch angle measurements that are not affected as much by stingwhip or other dynamic effects. At low Mach numbers there is little or no detectable stingwhip, but the errors are large at higher Mach numbers compared to the 0.01° level that constitutes the entire angle of attack error budget for precision wind tunnel testing such as performance testing. This explains why Mach number is indicated in the wind-on ANOVA table to be a highly significant factor in determining delta-pitch. The fact that the angle of attack dependence of delta-pitch varies in Figure 34 so dramatically with Mach number further reveals why the ANOVA table indicates large interactions between Mach number and the various-order terms in the AoA dependence.

Figure 35 compares delta-pitch for a variety of instruments at the highest Mach number tested – 0.9. Each instrument displays a different AoA dependence, as forecasted in the ANOVA table by the significant interactions between various AoA coefficients and instrument. These differences manifest themselves according to certain patterns, however. Note that for both of the video systems as well as the stingwhip-corrected inertial system, the variation in delta-pitch is small across all angles of attack between -4° and +10°, and relatively small in absolute terms as well. The variations are substantially larger for the uncorrected inertial systems and for the arc-sector corrected for sting bending, both common techniques in current widespread use for pitch-angle measurements. Errors in these latter systems approached a quarter degree – 25 times the error budget for angle of attack in typical precision wind tunnel tests.

1-CAMERA/2-CAMERA COMPARISON
Static laboratory tests were conducted to compare angle measurements made with the single camera solution (7) and angle measurements using 2-camera intersection. The 2-camera measurement system used

for these tests was developed for NASA by the High Technology Corporation[13]. The measurement system employs 2 progressive scan cameras with a resolution of 640 X 480. Software includes programs for image acquisition, target tracking, centroid calculation, camera calibration and 2-camera photogrammetric intersection. The centroid files output from each camera separately were used in an off-line reduction to produce the 2 sets of 1-camera results. A high-accuracy indexing table that has been calibrated to better than 1 arcsecond (0.0003°) was used as the standard. The pitch angle was varied over a range of −10° to 30° in 1° increments. A second indexing table was used to introduce roll angles of 0°, ±2°, and ±4° to assess the effect of an unknown roll on the angle data. No correction was made for the roll to simulate the case for wind tunnel models where an unknown roll may be present. Small roll angles are seen to introduce a zero-shift in the measured values. The 2-camera intersection results are presented in figure 36. For this figure and the following 2 plots, the known set angle is subtracted, leaving the angular error compared to the known standard. Figures 37 and 38 depict the single-camera results for the same 2 cameras as used to acquire the 2-camera intersection results. The same centroid data (image plane data) were used for the intersection results as for the two 1-camera solutions. Note the similarity of the 2-camera intersection and 1-camera result of camera #1. 1-Camera results for camera #2 are somewhat better than either the results using camera #1 or the results using both cameras. The excellent results found for camera #2 suggest that given the proper experimental situation, comparable or even better angular measurements can be made with a single camera than with 2-camera intersection. Summary results of the mean and standard deviation of the error (compared to the indexing table) are presented in Table III and figure 39.

Table III: Mean and std dev of error

	mean	std
2-camera	0.0136°	0.0138°
1-camera #1	0.0146°	0.0101°
1-camera #2	0.0033°	0.0028°

DYNAMIC EFFECTS
Both the videogrammetric technique and the commercially available Optotrak™ system have been evaluated to assess their immunity to dynamics as part of a series of tests conducted on the newly developed sting-whip corrected inertial devices[9]. A shaker at constant output level was varied from 0 to 70 Hz in small increments. The plate containing 6 LEDs used by the Optotrak system and 6 passive targets used by the videogrammetric system (figure 40) was excited in

AIAA 2001-0167. *39th AIAA Aerospace Sciences Meeting and Exhibit.* Reno, NV. Jan 2001.

12. DeLoach, R. "Tactical Defenses Against Systematic Variation in Wind Tunnel Testing" AIAA 2002-0885. *40th AIAA Aerospace Sciences Meeting & Exhibit.* January 14-17, 2002.

13. Liu, T., Radeztsky, R., Garg, S., and Cattafesta, L. "A Videogrammetric Model Deformation System and Its Integration with Pressure Paint", AIAA 99-0568, 1999.

14. Finley, T. D., *Private Communication*, NASA Langley Research Center, June 2002.
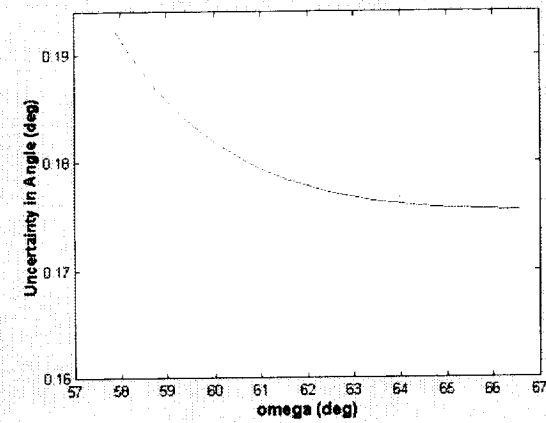
Figure 7. Uncertainty in angle as ω is varied.
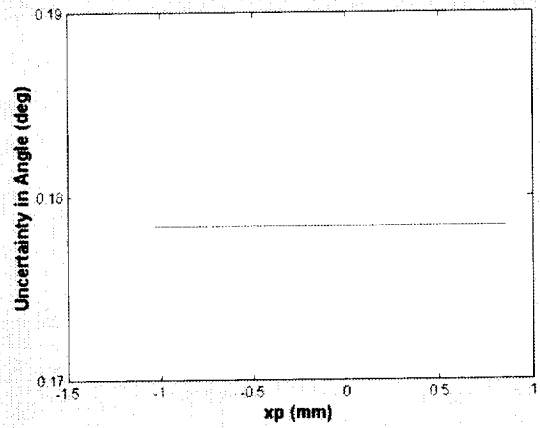
Figure 10. Uncertainty in angle as a function of x_p.
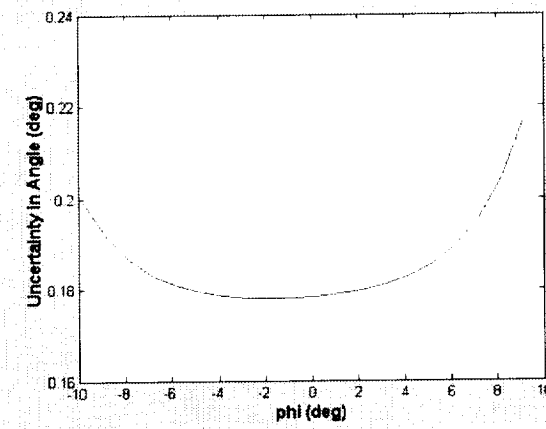
Figure 8. Uncertainty in angle as a function of ϕ.
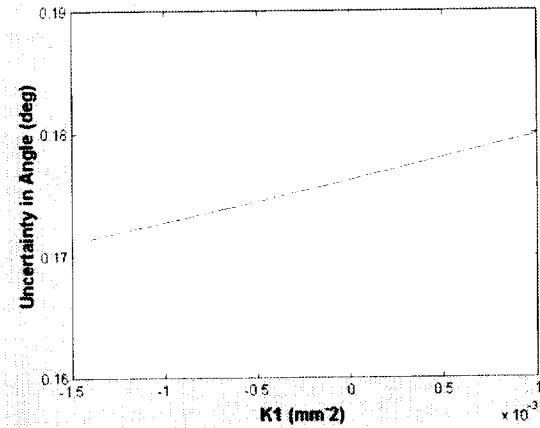
Figure 11. Uncertainty in angle as a function of K_1.
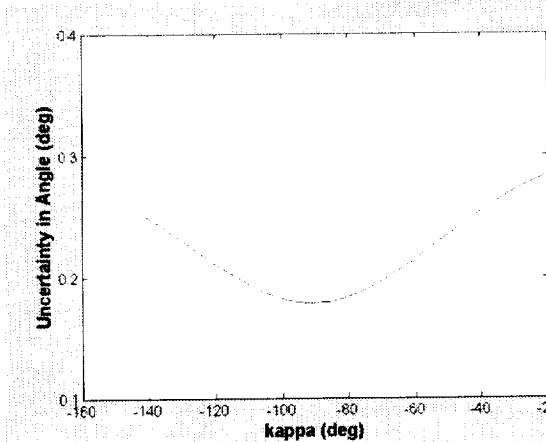
Figure 9. Uncertainty in angle as a function of κ.
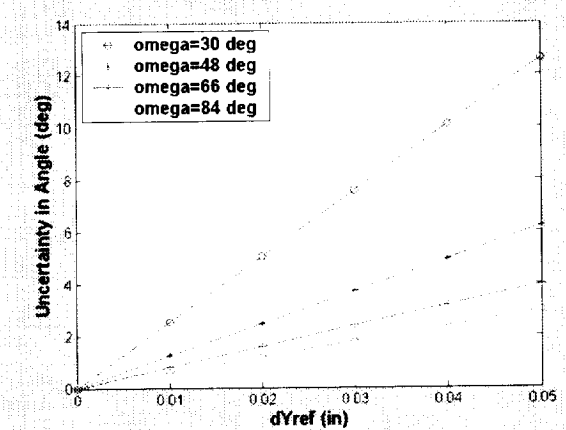
Figure 12. Uncertainty in angle as a function of error in Y_{ref}.
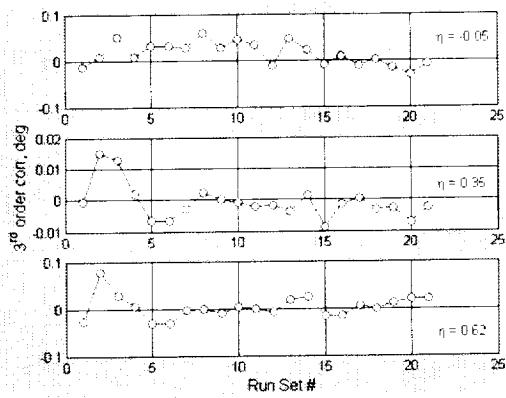
Figure 19. 3rd order correction at α = 6° as a function of run set number over 2.5 months for outboard semispan stations η.
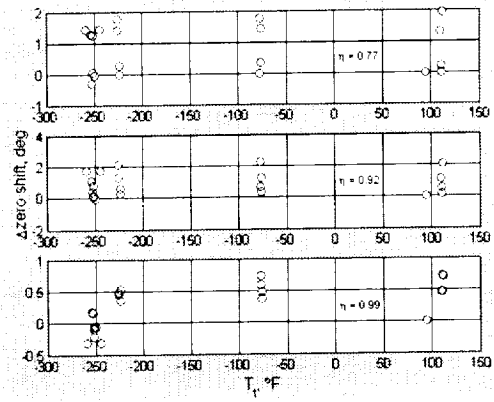
Figure 22. Δzero-shift as a function of T_t over 2.5 months for outboard semispan stations η.
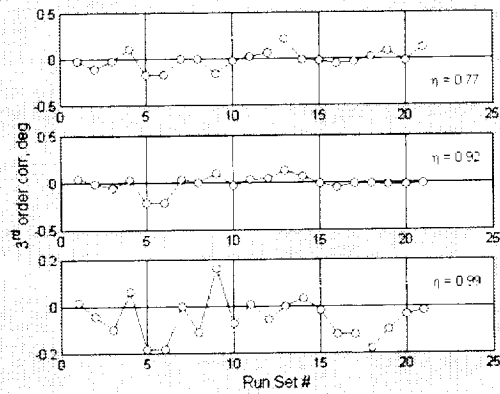
Figure 20. 3rd order correction at α = 6° as a function of run set number over 2.5 months for outboard semispan stations η.
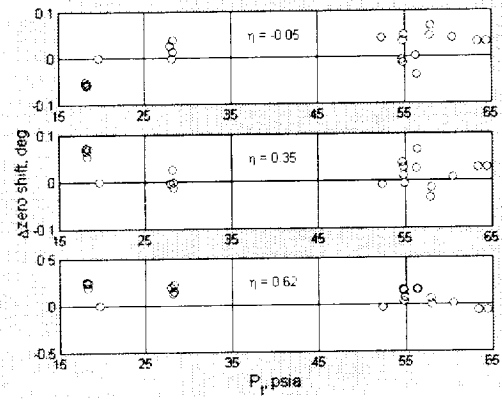
Figure 23. Δzero-shift as a function of P_t over 2.5 months for inboard semispan stations η.
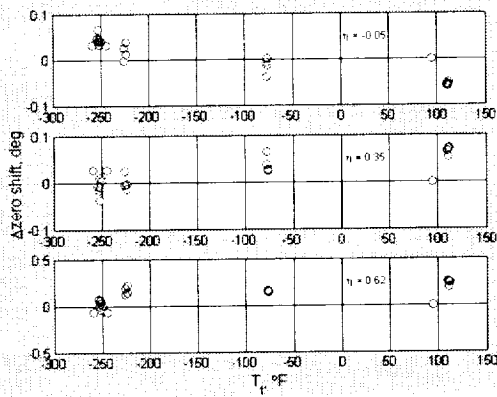
Figure 21. Δzero-shift as a function of T_t over 2.5 months for inboard semispan stations η.
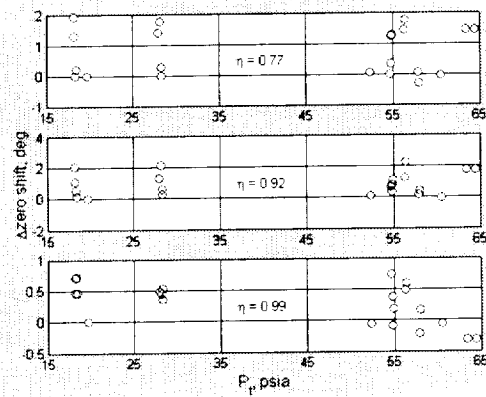
Figure 24. Δzero-shift as a function of P_t over 2.5 months for outboard semispan stations η.
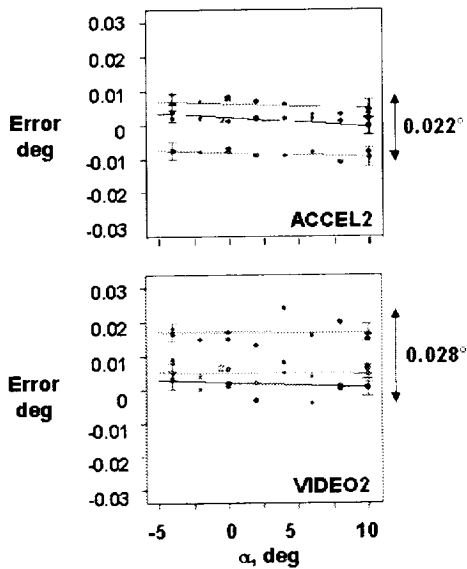
Figure 30. Error compared to AMS for accelerometer #2 and videogrammetric measurement #2, for three elapsed times throughout test.
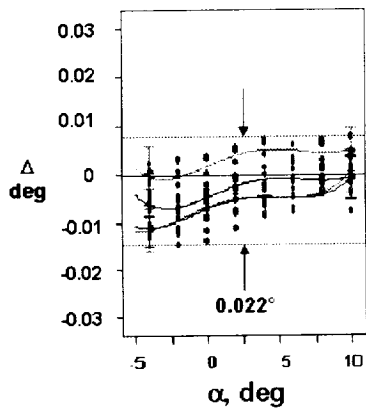
Figure 31. Differences, Δ, of the 1st corrected accelerometer measurements using the 2nd corrected accel as reference at M = 0.0, 0.3, 0.8, 0.9.
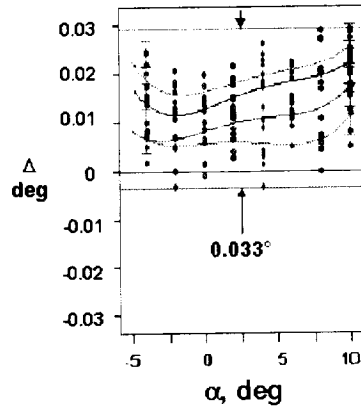
Figure 32. Differences, Δ, of the 1st videogrammetric measurements using the 2nd corrected accel as reference at M = 0.0, 0.3, 0.8, 0.9.
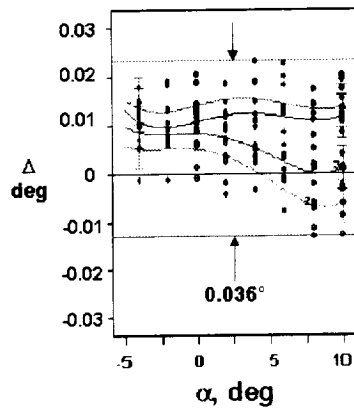
Figure 33. Differences, Δ, of the 2nd videogrammetric measurements using the 2nd corrected accel as reference at M = 0.0, 0.3, 0.8, 0.9.
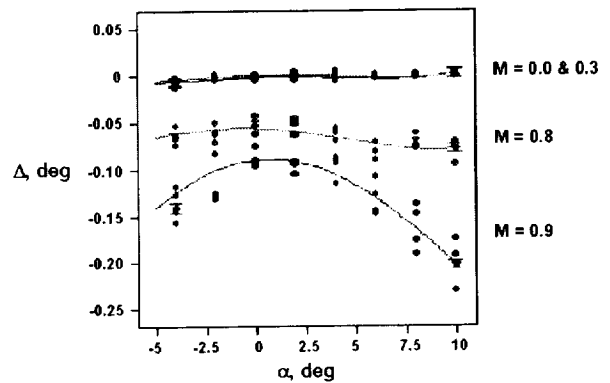
Figure 34. Accelerometer data uncorrected for sting whip dynamics at Mach 0, 0.3, 0.8, and 0.9.
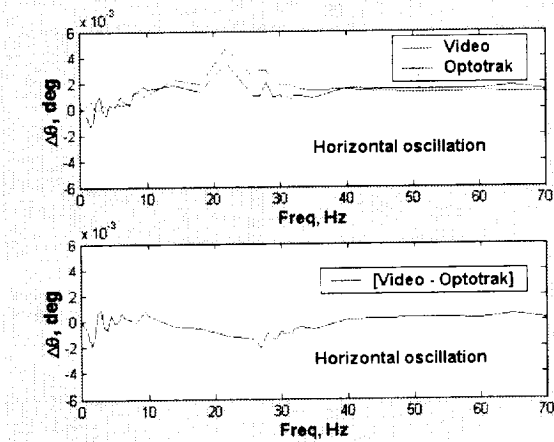
Figure 41. Change in angle as a function of horizontal oscillation frequency for videogrammetric and Optotrak angle measurements. Bottom plot is difference between video and Optotrak values.
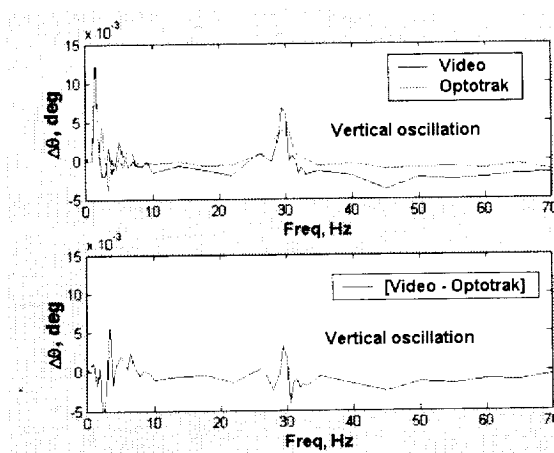
Figure 42. Change in angle as a function of vertical oscillation frequency for videogrammetric and Optotrak angle measurements. Bottom plot is difference between video and Optotrak values.